

SCIENTIFIC REPORTS



OPEN

Isotropic plasticity of β -type Ti-29Nb-13Ta-4.6Zr alloy single crystals for the development of single crystalline β -Ti implants

Received: 06 May 2016

Accepted: 23 June 2016

Published: 15 July 2016

Koji Hagihara¹, Takayoshi Nakano², Hideaki Maki², Yukichi Umakoshi² & Mitsuo Niinomi³

β -type Ti-29Nb-13Ta-4.6Zr alloy is a promising novel material for biomedical applications. We have proposed a 'single crystalline β -Ti implant' as new hard tissue replacements for suppressing the stress shielding by achieving a drastic reduction in the Young's modulus. To develop this, the orientation dependence of the plastic deformation behavior of the Ti-29Nb-13Ta-4.6Zr single crystal was first clarified. Dislocation slip with a Burgers vector parallel to $\langle 111 \rangle$ was the predominant deformation mode in the wide loading orientation. The orientation dependence of the yield stress due to $\langle 111 \rangle$ dislocations was small, in contrast to other β -Ti alloys. In addition, $\{332\}$ twin was found to be operative at the loading orientation around $[001]$. The asymmetric features of the $\{332\}$ twin formation depending on the loading orientation could be roughly anticipated by their Schmid factors. However, the critical resolved shear stress for the $\{332\}$ twins appeared to show orientation dependence. The simultaneous operation of $\langle 111 \rangle$ slip and $\{332\}$ twin were found to be the origin of the good mechanical properties with excellent strength and ductility. It was clarified that the Ti-29Nb-13Ta-4.6Zr alloy single crystal shows the "plastically almost-isotropic and elastically highly-anisotropic" nature, that is desirable for the development of 'single crystalline β -Ti implant'.

Ti alloys are some of the most attractive and widely used biomedical implant materials^{1,2}. They are generally preferred to 316L stainless steel and Co-Cr-Mo alloys owing to their low weight, excellent biocompatibility, corrosion resistance, high specific strength, and low elastic modulus³. Among these properties, control of the Young's modulus has been important in the recent development of implant materials. A reduction in Young's modulus is essential to prevent bone degradation and bone resorption, caused by the difference in the Young's moduli between a bone replacement material and natural human bone, i.e. the stress shielding by the implant⁴. Among the Ti alloys, the Ti-6Al-4V alloy with an $\alpha + \beta$ two-phase microstructure is currently widely used as an implant material. The Young's modulus of the Ti-6Al-4V alloy is ~ 110 GPa, approximately half of that of 316 stainless steel or Co-Cr-Mo alloys^{2,3}. However, the Young's modulus is still significantly higher than that of the cortical bone in humans (~ 10 – 30 GPa)⁵. In addition, studies considering the long-term health problems caused by Al and V ion release from Ti-6Al-4V have been reported⁶. Thus, novel Ti alloys with lower Young's moduli and improved biocompatibility are required. Recently, β (bcc)-type Ti-Nb-Ta-Zr quaternary alloys containing only non-toxic bcc-stabilized elements (Nb and Ta) have received growing interest^{7–12}, as β -Ti alloys generally exhibit lower Young's moduli than α -Ti alloys, and their processabilities are also better owing to their higher crystal symmetry.

Among the β -Ti alloys, Niinomi *et al.* reported a new alloy, namely Ti-29Nb-13Ta-4.6Zr (mass%)⁹, which exhibits a lower Young's modulus of ~ 65 GPa¹⁰. Thus, the Ti-29Nb-13Ta-4.6Zr alloy is considered a novel class of implant material that has undergone significant development^{9–12}. However, its Young's modulus remains higher than that of human bone, and so further research is still required. The control of the implant's inner structure, for example the introduction of a porous structure, is considered as one of the approaches for the further reduction of the Young's

¹Department of Adaptive Machine Systems, Graduate School of Engineering, Osaka University, 2-1 Yamadaoka, Suita, Osaka 565-0871, Japan. ²Division of Materials and Manufacturing Science, Graduate School of Engineering, Osaka University, 2-1 Yamadaoka, Suita, Osaka 565-0871, Japan. ³Institute for Materials Research, Tohoku University, 2-1-1 Aoba-ku, Sendai, Miyagi 980-8577, Japan. Correspondence and requests for materials should be addressed to T.N. (email: nakano@mat.eng.osaka-u.ac.jp)

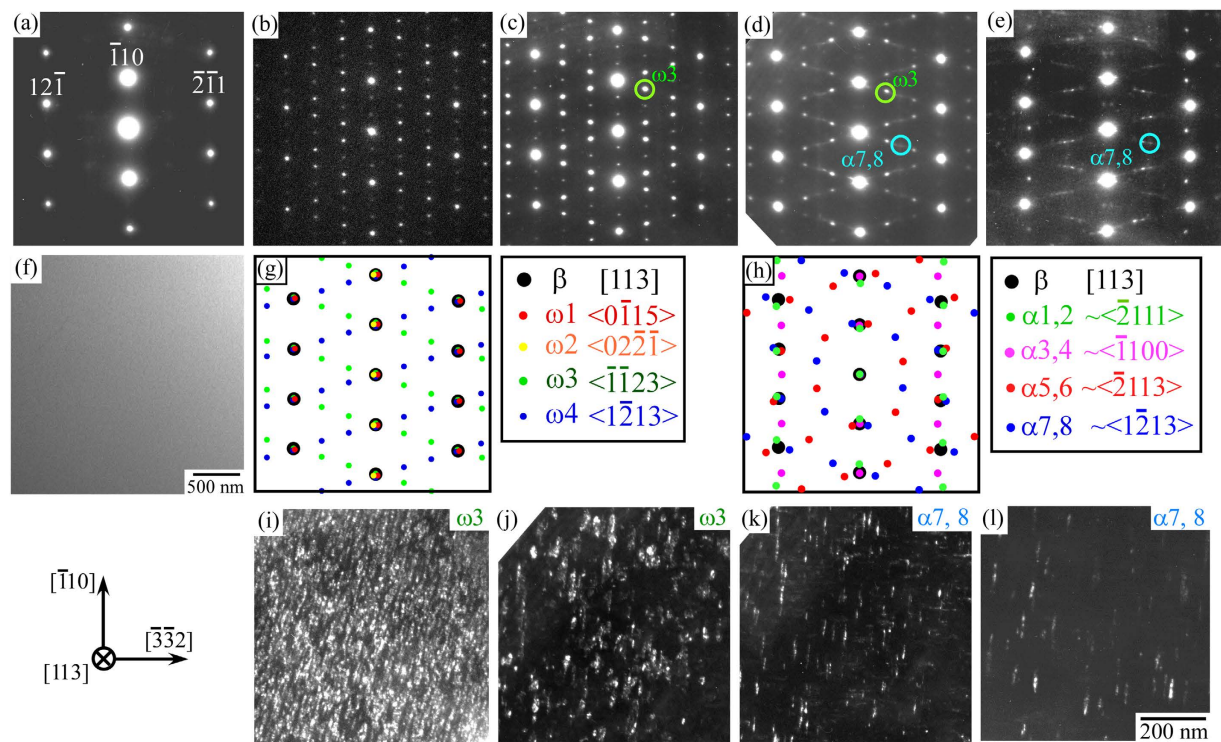


Figure 1. Variations in microstructure with heat treatment examined by TEM. (a–e) SAED patterns of the Ti-29Nb-13Ta-4.6Zr single crystal observed along the [113] direction, in specimens of (a) as-ST specimen, and annealed at (b) 573 K, (c) 598 K, (d) 673 K, and (e) 723 K for 259.2 ks, respectively. (f) Bright-field image of the as-ST specimen. (g,h) Simulated diffraction patterns derived from (g) ω -phase and (h) α -phase precipitates with distinct orientation relationships with respect to the β -matrix phase. (i–l) Dark-field images of the (i) precipitated ω -phases in the specimen annealed at 598 K for 259.2 ks, (j,k) precipitated ω -phases and α -phases in the specimen annealed at 673 K for 259.2 ks, and (l) precipitated α -phases in the specimen annealed at 723 K for 259.2 ks. The reflection spots observed for dark-field images are indicated as circles in Fig. 1(c–e).

modulus of the implant¹³. However, there still exists an argument to use a porous implant for some applications where a large load is applied (e.g., artificial hip joints) in terms of the reliability of its mechanical properties.

Our group proposed a novel approach for lowering the Young's modulus of the material itself, namely the use of the single crystal. The Young's modulus in crystals is known to show orientation dependence even in the bcc-structured crystal exhibiting high crystal symmetry, and so it may be possible to reduce the Young's modulus in the implant using the single crystal. In order to validate this concept, we examined the anisotropy of the elastic properties of the Ti-29Nb-13Ta-4.6Zr alloy using the single crystal^{14,15}. A strong orientation dependence of the Young's modulus was indeed confirmed, with the Young's modulus exhibiting its highest value (~80 GPa) along the $\langle 111 \rangle$ orientation, and its lowest value along the $\langle 001 \rangle$ orientation (~35 GPa). The lowest Young's modulus along the $\langle 001 \rangle$ orientation is close to that of cortical human bones (~10–30 GPa). These results imply the feasibility of using 'single crystalline β -Ti implant' as new hard tissue replacements for suppressing the stress shielding by the implant.

For the development of the 'single crystalline implant', not only the elastic properties but also the control of mechanical properties is important. For example, strength and resistance to fracture and fatigue should be sufficiently high. Studies have shown that the plastic deformation behavior also shows an orientation dependence in β -Ti alloys^{16–18}. Although many reports exist on the mechanical properties of the Ti-29Nb-13Ta-4.6Zr alloy in a polycrystalline form^{9–12}, our preliminary single crystal report appears to be the only one published to date¹⁹. Thus, the orientation dependence of the plastic deformation behavior of Ti-29Nb-13Ta-4.6Zr has not yet been fully investigated. In addition, the mechanical properties of β -Ti alloys vary significantly with heat treatment^{2,18}. This has also been reported for the Ti-29Nb-13Ta-4.6Zr alloy²⁰, although details were not sufficiently elucidated yet. We, therefore, chose to investigate the plastic deformation behavior of a Ti-29Nb-13Ta-4.6Zr biomedical implant alloy single crystal, and focusing on its orientation dependence and the influence of microstructure. From the results, the possibility of the development of the 'single crystalline β -Ti implant' by using the Ti-29Nb-13Ta-4.6Zr alloy single crystal was discussed.

Results

Relation between the microstructure and mechanical properties of the Ti-29Nb-13Ta-4.6Zr alloy single crystal. To control the mechanical properties of the β -Ti alloys, control of the microstructure by heat treatment is useful. To achieve this, variations in the microstructure depending on the heat treatment conditions were first examined in the Ti-29Nb-13Ta-4.6Zr single crystal. Figure 1(a–e) show the variation in the

selected area electron diffraction (SAED) patterns observed along the [113] direction upon heat treatment, in the original as- solution-treated (ST) single-crystalline specimen and those annealed at 573, 598, 673, and 723 K for 259.2 ks. As shown in Fig. 1(a), only the diffraction spots derived from the β -phase with a bcc structure were clearly observed in the ST specimen, demonstrating that the ST single crystal was composed of a β -single-phase, as is also confirmed by the bright field image shown in Fig. 1(f). In contrast, a number of additional spots were observed in the annealed specimens, as shown in Fig. 1(b–e). The positions and intensities of the extra spots varied with annealing temperature, suggesting that different phases precipitated at different temperatures. The precipitates present in the β -matrix-phase are supposed to be either a ω -phase with a hexagonal unit cell, or an α -phase with a hexagonal close-packed (hcp) unit cell. It is generally known that these phases precipitate with distinct relationships to the β -Ti matrix phase as follows:

$$\omega - \text{phase: } \{111\}_{\beta} // \{0001\}_{\omega}, \quad \langle 1\bar{1}0 \rangle_{\beta} // \langle 11\bar{2}0 \rangle_{\omega} \quad (1)$$

$$\alpha - \text{phase: } \{1\bar{1}0\}_{\beta} // \{0001\}_{\alpha}, \quad \langle 111 \rangle_{\beta} // \langle 11\bar{2}0 \rangle_{\alpha} \quad (2)$$

According to these relationships, four equivalent variants are considered for the ω -precipitates, and 12 variants are considered for the α -precipitates (see Supplementary Table S1). Taking their crystallographic orientations into consideration, Fig. 1(g,h) show the calculated SAED patterns from the precipitated ω - and α -phase variants in the β -matrix-phase when observed along $[113]_{\beta}$. As only eight net diffraction patterns with relatively low lattice indices among the 12 variants were indicated for the simulated α -phase diffraction pattern in Fig. 1(h), the observed TEM diffraction patterns could not be perfectly reproduced. However, by comparing to the experimental SAED patterns, it was elucidated that the specimens were composed of a $\beta + \omega$ two-phase at 573 K and 598 K, a $\beta + \omega + \alpha$ three-phase at 673 K, and a $\beta + \alpha$ two-phase at 723 K. This was further confirmed by dark-field observations. Figure 1(i) show the dark field images observed in the specimen annealed at 598 K, with the circled spots shown in Fig. 1(c). Using the spot, the ω -phases were confirmed to be densely precipitated in the specimen. The ω -phases exhibited ellipse-like shapes, having the long axis aligned along the $[0001]$ direction, with an average length of ~ 10 nm. Figure 1(j,k) show the dark-field images of the specimen annealed at 673 K. With the same spot used for observation in Fig. 1(i), the presence of ω -precipitates was confirmed as shown in Fig. 1(j). In addition, using the spot named “ $\alpha 7,8$ ” in Fig. 1(d), the precipitation of the α -phase was also observed as shown in Fig. 1(k). The α -phases precipitated abundantly with thin plate-like shapes. In the specimen annealed at 723 K, α -phase precipitates were confirmed to be slightly coarser, but maintained their plate-like shape, as shown in Fig. 1(l).

The change in mechanical properties of the Ti-29Nb-13Ta-4.6Zr alloy single crystal following heat treatment was examined by compression tests at a $[\bar{1}49]$ loading orientation, where the Schmid factor for $(\bar{1}01)[111]$ is 0.500, as shown in Table 1. Figure 2(a) shows the typical stress-strain curves of the specimens deformed at a $[\bar{1}49]$ loading orientation. Furthermore, Fig. 2(b) shows the variations in yield stress and homogeneous plastic strain before fracture, both as a function of annealing temperature. The yield stress monotonously increased with increasing annealing temperature, while the strengthening behavior was largely divided into two temperature regions. Between 573 and 598 K, where only the ω -phase precipitated, alloy strengthening was relatively small, approximately less than 150 MPa. However, at increased temperatures (673–723 K) where the α -phase also precipitated, the stress increase was pronounced, to more than 300 MPa. Accompanying the increase in yield stress, the fracture strain decreased rapidly with rising annealing temperature. Focusing on the shape of the stress-strain curve, the ST specimen exhibited no work hardening after yielding. The flow stress showed a gradual decrease as deformation proceeded, but over 30% plastic strain could be obtained before fracture. With an increase in the annealing temperature, the steady flow stress region after yielding was shorter, and thus, the fracture strain decreased. In the specimens annealed above 598 K, where a large amount of α -phase was precipitated, the fracture strain was decreased lower than 10%.

Figure 2(c–g) shows the morphology of the deformation markings introduced in the specimens by deformation at a $[\bar{1}49]$ loading orientation to $\sim 2\%$ plastic strain, observed on the $(11\bar{5}\bar{1})$ surface. The features of the deformation traces suggest that the dislocation slip carried the strain in deformation, and other deformation modes were not observed irrespective of the heat treatment condition. By the two-face slip trace analysis, the slip plane of the dislocations was confirmed to be macroscopically parallel to $(\bar{1}01)$. From the consideration based on the Schmid factor shown in Table 1, the primary operative slip system was expected to be $(\bar{1}01)[111]$. This was confirmed by the transmission electron microscopy (TEM) observation, as described later. In addition, the $(101)[\bar{1}\bar{1}1]$ slip was locally observed as a secondary slip system. It should be noted that although the traces of primary slip were aligned macroscopically parallel to $(\bar{1}01)$, they were not straight. The slip traces exhibited a wave-like form in all specimens. This suggests that the $[111]$ dislocations frequently cross-slip from the $(\bar{1}01)$ plane to other planes.

Although the $(\bar{1}01)[111]$ slip was confirmed in all specimens, the detailed morphology of the slip traces varied under different heat treatment conditions. In the ST specimen, slip traces were relatively homogeneously distributed over the specimen surface. However, in the specimens annealed at 573 K and 598 K, the slip traces were coarsely introduced. The contrast of the traces became stronger with the concentration of slip traces, resulting in the formation of slip bands. Between the strong slip bands, no fine slip trace was observed. The formation of microcracks was occasionally observed along the slip bands, leading to a decrease in specimen ductility. Interestingly, at annealing temperatures above 673 K, the slip traces were once again introduced homogeneously, and the contrast became weak. In the specimen annealed at 723 K the slip traces were too faint to accurately determine the slip plane.

Deformation mode	Slip (twinning) system	Schmid factors				
		$[\bar{1}451]$ ($\chi = -25^\circ$)	$[\bar{1}418]$ ($\chi = -15^\circ$)	$[\bar{1}49]$ ($\chi = 0^\circ$)	$[\bar{1}45.8]$ ($\chi = 15^\circ$)	$[\bar{1}44.5]$ ($\chi = 25^\circ$)
{110} <111> slip	$(\bar{1}01)[111]$	0.438	0.479	0.500	0.483	0.453
	$(101)[\bar{1}11]$	0.437	0.469	0.467	0.419	0.366
	$(\bar{1}01)[1\bar{1}1]$	0.373	0.293	0.167	0.045	0.028
	$(101)[11\bar{1}]$	0.374	0.303	0.200	0.109	0.059
	$(\bar{1}10)[111]$	0.042	0.128	0.250	0.353	0.410
	$(110)[\bar{1}11]$	0.026	0.084	0.175	0.260	0.311
	$(110)[1\bar{1}1]$	0.022	0.047	0.050	0.020	0.015
	$(\bar{1}10)[11\bar{1}]$	0.037	0.091	0.125	0.113	0.083
	$(0\bar{1}1)[111]$	0.396	0.350	0.250	0.129	0.043
	$(0\bar{1}1)[\bar{1}11]$	0.410	0.384	0.292	0.159	0.055
	$(011)[1\bar{1}1]$	0.395	0.340	0.217	0.065	0.044
	$(011)[11\bar{1}]$	0.412	0.394	0.325	0.223	0.142
{112} <111> slip	$(112)[\bar{1}\bar{1}1]$	0.454	0.403	0.303	0.192	0.116
	$(\bar{1}12)[1\bar{1}1]$	0.443	0.366	0.221	0.064	0.042
	$(1\bar{1}2)[\bar{1}11]$	0.489	0.492	0.438	0.333	0.243
	$(11\bar{2})[\bar{1}\bar{1}\bar{1}]$	0.481	0.479	0.433	0.354	0.289
	$(121)[\bar{1}1\bar{1}]$	0.240	0.224	0.154	0.049	0.034
	$(\bar{1}21)[11\bar{1}]$	0.259	0.280	0.260	0.194	0.130
	$(1\bar{2}1)[\bar{1}\bar{1}\bar{1}]$	0.204	0.128	0.000	0.129	0.211
	$(12\bar{1})[\bar{1}11]$	0.222	0.173	0.067	0.059	0.148
	$(211)[1\bar{1}\bar{1}]$	0.267	0.319	0.370	0.392	0.391
	$(\bar{2}11)[\bar{1}\bar{1}\bar{1}]$	0.277	0.350	0.433	0.483	0.498
	$(2\bar{1}1)[11\bar{1}]$	0.194	0.122	0.043	0.002	0.014
	$(21\bar{1})[1\bar{1}1]$	0.203	0.142	0.067	0.015	0.007
{332} <113> twin	$(332)[11\bar{3}]$	0.409 ^c	0.433 ^c	0.425 ^c	0.377 ^c	0.328 ^c
	$(\bar{3}32)[\bar{1}1\bar{3}]$	0.425 ^c	0.472 ^c	0.476 ^c	0.420 ^c	0.354 ^c
	$(3\bar{3}2)[1\bar{1}\bar{3}]$	0.338 ^c	0.230 ^c	0.063 ^c	0.095 ^t	0.189 ^t
	$(\bar{3}\bar{3}2)[\bar{1}\bar{1}\bar{3}]$	0.356 ^c	0.288 ^c	0.177 ^c	0.069 ^c	0.002 ^c
	$(323)[1\bar{3}1]$	0.147 ^t	0.053 ^t	0.084 ^c	0.203 ^c	0.270 ^c
	$(\bar{3}23)[\bar{1}\bar{3}1]$	0.161 ^t	0.083 ^t	0.050 ^c	0.186 ^c	0.273 ^c
	$(3\bar{2}3)[113]$	0.216 ^t	0.235 ^t	0.210 ^t	0.138 ^t	0.069 ^t
	$(\bar{3}\bar{2}3)[\bar{1}31]$	0.233 ^t	0.288 ^t	0.317 ^t	0.297 ^t	0.258 ^t
	$(233)[\bar{3}11]$	0.232 ^t	0.304 ^t	0.388 ^t	0.445 ^t	0.466 ^t
	$(\bar{2}33)[113]$	0.213 ^t	0.244 ^t	0.269 ^t	0.271 ^t	0.261 ^t
	$(2\bar{3}3)[\bar{3}\bar{1}1]$	0.171 ^t	0.127 ^t	0.068 ^t	0.021 ^t	0.002 ^t
	$(\bar{2}\bar{3}3)[3\bar{1}1]$	0.154 ^t	0.090 ^t	0.022 ^t	0.011 ^c	0.015 ^c

Table 1. Schmid factors for possible deformation modes at the five examined loading orientations. The superscript t and c indicate the deformation twins operative in the tensile and compressive deformation, respectively.

The dislocation structures introduced in the specimens were examined by TEM. Figure 3(a) shows the dislocation structure of the ST specimen composed of a β -single phase, observed on the $(\bar{1}01)$ slip plane. Relatively straight morphologies of the dislocations were abundantly observed. By g·b contrast analysis, the Burgers vector of the dislocations was confirmed to be parallel to $[111]$. The crystal orientations examined by SAED pattern analysis are indicated in the figures. They show that the aligned directions of the dislocations were almost parallel to $[111]$, indicating that the observed dislocations are predominantly screw dislocations. Figure 3(b,c) show the dislocations observed in the 573 K and 598 K annealed specimens, respectively, where ω -phases precipitated in the β -matrix phase. As the same as that observed in the ST specimen, the Burgers vectors of the dislocations were parallel to $[111]$, and they predominantly exhibited screw characteristics. However, in the 573 K and 598 K annealed specimens, the dislocation segments were shorter, and were curled in comparison to those in the ST specimen. This variation demonstrates that precipitation of the ω -phase significantly affected the motion of the $[111]$ dislocation. TEM observation was also conducted in the deformed specimen annealed at 673 K and 723 K. In those specimens, however, the dislocation structure could not be sufficiently examined since the images of the

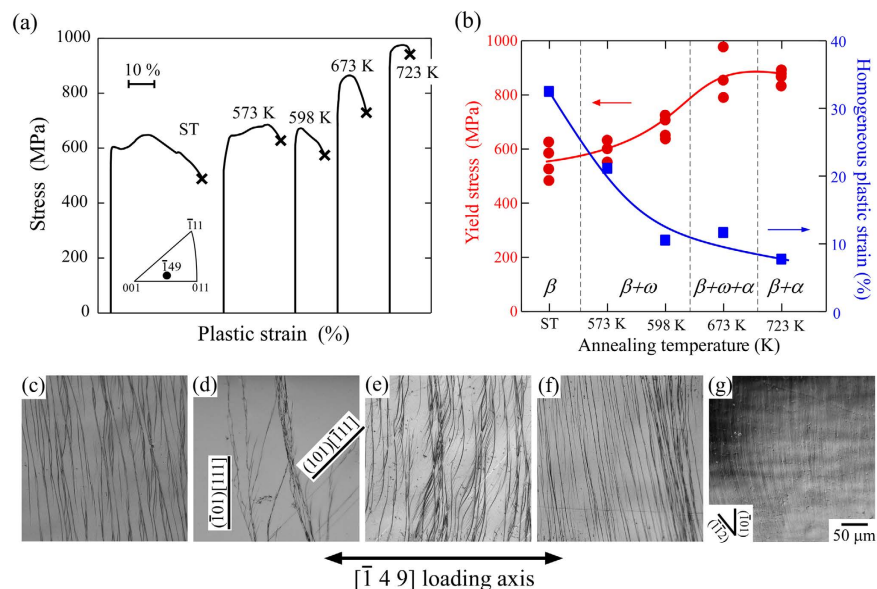


Figure 2. Variations in deformation behaviors with heat treatment. (a) Variations in typical stress-strain curves of the Ti-29Nb-13Ta-4.6Zr single crystals deformed at $[\bar{1}49]$ orientation, with heat treatment. (b) Corresponding variations in yield stress (0.2% offset stress) and homogeneous plastic strain as a function of the annealing temperature. (c–g) Optical micrographs showing the variations in morphology of the slip traces with heat treatment, introduced in the specimens deformed at $[\bar{1}49]$ loading orientation to $\sim 2\%$ plastic strain. (c) as-ST specimen, and the specimens annealing at (d) 573 K, (e) 598 K, (f) 673 K, and (g) 723 K, respectively. The surface planes of the observed specimens are parallel to $(11\bar{1})$.

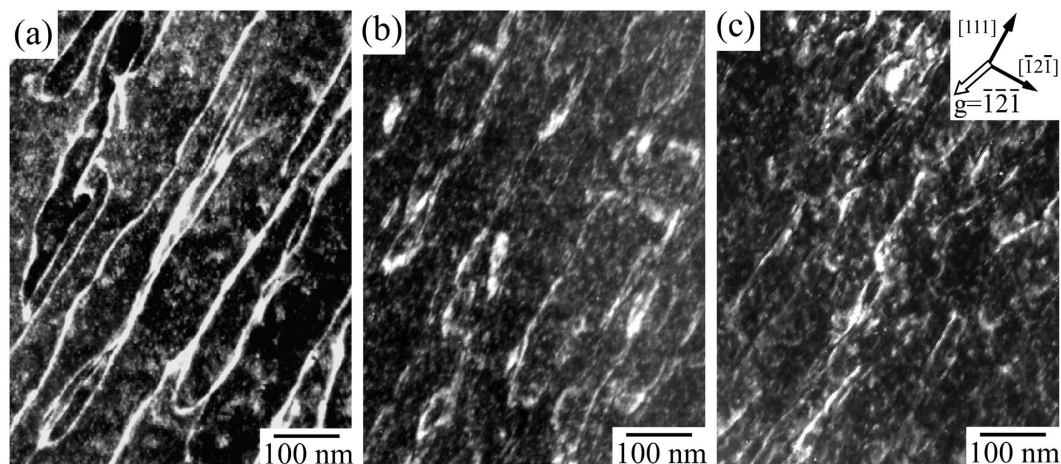


Figure 3. Dislocation structure in specimens deformed to $\sim 2\%$ plastic strain at $[\bar{1}49]$ loading orientation. (a) As-ST specimen, (b) annealed at 573 K, and (c) annealed at 598 K. Foil $// (10\bar{1})$ slip plane, and the observed beam direction (B) $// [\bar{1}01]$.

dislocations were faint owing to the presence of large amounts of α -phases as shown in Fig. 1(k,l). In those specimens the slip traces became anomalously faint, as shown in Fig. 2(f,g).

Orientation dependence of the plastic deformation behavior. To examine the orientation dependence of the plastic deformation behavior of Ti-29Nb-13Ta-4.6Zr alloy, specimens with five different loading axes, including the $[\bar{1}49]$ orientation, were prepared on the $[410]$ zone axis in a $[001]$ - $[011]$ - $[\bar{1}11]$ standard triangle, as shown in Fig. 4(m), and their plastic deformation behaviors were compared. The five loading axes chosen were parallel to $[\bar{1}451]$, $[\bar{1}418]$, $[\bar{1}49]$, $[\bar{1}458]$, and $[\bar{1}445]$. In the bcc-structured crystal, the angle between the maximum resolved shear stress plane (MRSSP) in the $[111]$ zone and the reference $(\bar{1}01)$ plane, defined as “ χ ” is important in governing the orientation dependence of the plastic deformation behavior. In this aspect, the loading axes selected in this study correspond to $\chi = -25^\circ$ at $[\bar{1}451]$, $\chi = -15^\circ$ at $[\bar{1}418]$, $\chi = 0^\circ$ at $[\bar{1}49]$, $\chi = +15^\circ$ at $[\bar{1}458]$, and $\chi = +25^\circ$ at $[\bar{1}445]$ as shown in Fig. 4(m).

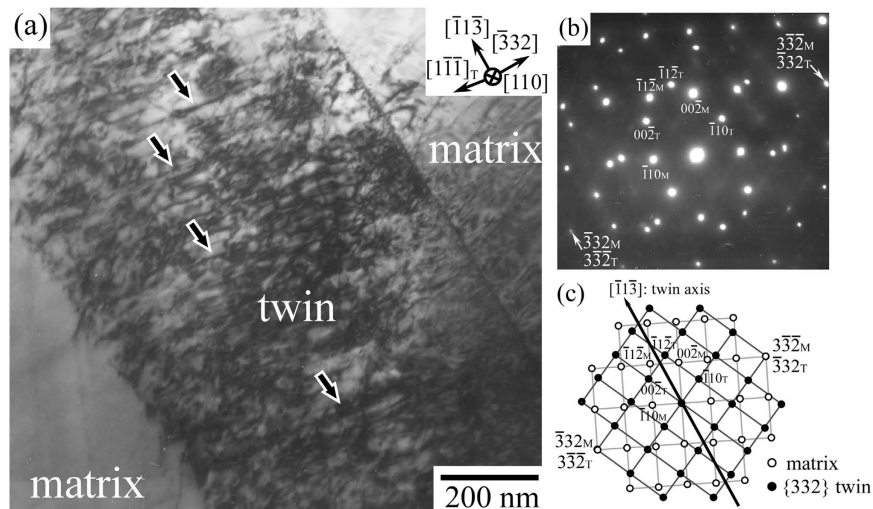


Figure 5. Observation of {332} twin by TEM. (a) Bright-field TEM image observed in the as-ST specimen deformed at $[\bar{1} \ 4 \ 51]$ ($\chi = -25^\circ$) to $\sim 2\%$ plastic strain. Observed beam direction is parallel to $[110]$. (b) SAED pattern obtained at the boundary of the band-like deformation product. (c) Corresponding key diagram. Analysis of the SAED pattern demonstrates that the band-like deformation product is the $(\bar{3}32)[\bar{1}1\bar{3}]$ deformation twin.

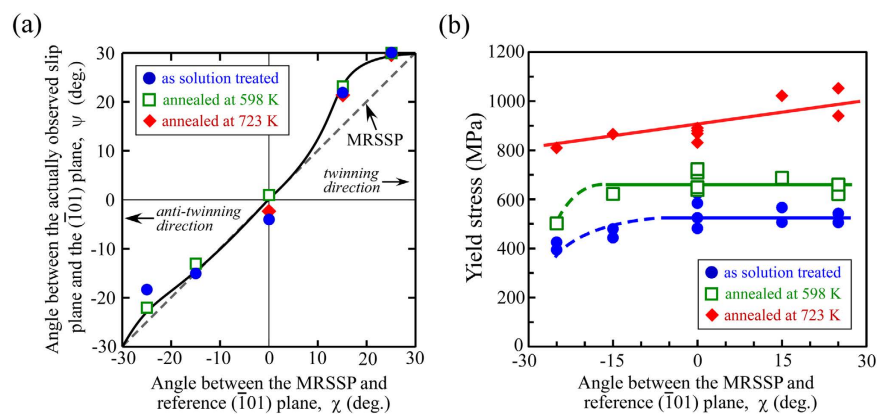


Figure 6. Orientation dependence of the deformation behavior. (a) Variations in the slip plane of $[111]$ dislocations with loading orientation; the so-called ψ – χ curve measured in the Ti-29Nb-13Ta-4.6Zr single crystal compressed at RT. (b) Corresponding orientation dependence of the yield stress examined.

orientation, irrespective of the heat-treatment condition. However, in the specimen annealed at 723 K, the slip planes could not be determined precisely at the $[\bar{1} \ 4 \ 51]$ and $[\bar{1} \ 4 \ 18]$ loading orientations because of the faint slip traces.

In order to discuss quantitatively the variations in the slip plane, ψ – χ curve analysis was conducted, and the results are summarized in Fig. 6(a). The χ is defined as the angle between the MRSSP in the $[111]$ zone and the reference $(\bar{1}01)$ plane, which varies depending on the loading axis, as shown in Fig. 4(m). Furthermore, ψ is the angle between the actually observed slip plane and the $(\bar{1}01)$ plane. If the slip plane does not vary from $(\bar{1}01)$ in any loading orientation, a horizontal line can be drawn along $\psi = 0$, whereas if the slip plane freely varies depending on the resolved shear stress, it will vary along the dashed line shown in Fig. 6(a), which corresponds to the MRSSP (i.e., $\psi = \chi$). It was found experimentally that the slip plane generally varied along the MRSSP, although a selection of slip traces showed a slight deviation from the MRSSP at $\chi \geq 15^\circ$. The observed slip plane moved from the MRSSP to $(\bar{2}11)$ at $\chi \geq 15^\circ$.

Figure 6(b) shows the variation in yield stress with the loading axis defined by the χ -value, focused for five loading orientations on the $[410]$ zone axis. As shown in Fig. 2(b), the yield stress increased with annealing, with a larger increase upon annealing at 723 K compared to 598 K at the $[\bar{1}49]$ orientation ($\chi = 0^\circ$). Similar observation were made at all loading orientations. It should be noted that the yield stress gave comparable values at all loading orientations in the ST specimens, i.e., the yield stress showed little orientation dependence, except for that at $\chi = -25^\circ$. At around $\chi = -25^\circ$, however, the yield stress slightly decreased compared to other loading orientations. Almost similar orientation dependence of the yield stress was observed in the specimens annealed at 598 K.

Note that the loading orientations where the slight decreases in yield stress were observed correspond to the regions where {332} twins formed in compression tests, as shown in Fig. 4. On the other hand, the yield stress of the specimens annealed at 723 K show a slight decrease as decreasing in the χ -value, although the formation of deformation twin was not observed in them.

Discussion

We found that the plastic deformation behavior of the solution-treated Ti-29Nb-13Ta-4.6Zr alloy single crystal was considerably isotropic and the orientation dependence of the yield stress was small, particularly in the loading orientations where $\langle 111 \rangle$ dislocations are operative, as shown in Fig. 6(b). This differed from the behavior of the Ti-15Mo-5Zr-3Al β -phase single crystal, which is another promising material for use in biomedical implant applications, as approved by the International Organization for Standardization (ISO). As previously reported²¹, the yield stress of the Ti-15Mo-5Zr-3Al single crystal showed a relatively strong orientation dependence, increasing with a decrease in χ . Thus, the compressive yield stress is lower at the loading orientation where the $(\bar{2}11)$ [111] slip is preferentially operative (the twinning sense direction) than where the $(\bar{1}\bar{1}2)$ [111] slip is preferential (anti-twinning sense direction). The compressive yield stress at $\chi = -25^\circ$ was approximately 1.2 times higher than that at $\chi = 25^\circ$ in Ti-15Mo-5Zr-3Al. In contrast, the compressive yield stress in Ti-29Nb-13Ta-4.6Zr was comparable at all orientations except for those at approximately $\chi = -25^\circ$, where the formation of {332} twins occurred. These different features of the plastic deformation behavior in the bcc-structured β -Ti crystals must be derived from the variation in the non-planar dislocation core structure of the $\langle 111 \rangle$ dislocation, as discussed previously²¹. In Ti-15Mo-5Zr-3Al, the $\langle 111 \rangle$ dislocation may exhibit a more complicated three-dimensional dislocation core structure that induces the twinning/anti-twinning sense asymmetry in the dislocation motion when compared to Ti-29Nb-13Ta-4.6Zr. Indeed, in Ti-15Mo-5Zr-3Al, the transition behavior of the slip plane largely deviated from the MRSSP towards $(\bar{2}11)$ ²¹. We proposed that such variations in the plastic deformation behavior of multi-component β -Ti alloys are predominantly affected by the properties of the major bcc-phase stabilizing constituent element itself, in this case Nb and Mo, respectively. This hypothesis is derived from the studies of Duesbery and Vitek²². They studied the plastic deformation behavior of various pure bcc metals, and found that plastic anisotropy is more stronger in group VIB metals (Mo and W) than in group VB metals (Nb and Ta)²². This is in agreement with the behavior of the Ti-15Mo-5Zr-3Al and Ti-29Nb-13Ta-4.6Zr systems. In addition, Hanada reported that the plastic deformation behavior of a Ti-Nb binary single crystal (Ti-52wt.%Nb) showed little orientation dependence at 300 K¹⁸, a property also observed in our Ti-29Nb-13Ta-4.6Zr crystal. However, Hanada also reported that the Ti-Nb binary single crystal exhibits strong anisotropic deformation behavior when the deformation temperature was decreased to 77 K. This suggests that the anisotropic feature of the plastic behavior in the β -Ti crystal is controlled by both the alloy composition and the deformation temperature. The effect of temperature can be explained by the temperature dependence of the thermal activation process for the transformation of the three-dimensional non-planar dislocation core structure to the mobile planar structure. Further studies using single crystals are required to clarify details regarding the controlling factor of the plastic deformation behavior of multi-element β -Ti alloys.

As described above, the yield stress of the solution-treated Ti-29Nb-13Ta-4.6Zr crystal shows little orientation dependence in the wide loading orientation region where the operation of $\langle 111 \rangle$ dislocations are dominant. However, in the ST specimen the yield stress slightly decreased at around $-25^\circ \leq \chi \leq -15^\circ$. In the specimens exhibiting lower yield stress, the formation of {332} twins was observed, as shown in Fig. 4(a,b). The slight decrease in yield stress at approximately $\chi = -25^\circ$ must, therefore, be ascribed to the operation of the {332} twins. In the deformed specimen at $[\bar{1} \ 4 \ 18]$ ($\chi = -15^\circ$) and $[\bar{1} \ 4 \ 51]$ ($\chi = -25^\circ$) loading orientations, the formation of $(\bar{3}32)$, $(\bar{3}\bar{3}2)$, (332) , and $(3\bar{3}\bar{2})$ twins were confirmed among the twelve {332} twinning systems. As shown in Table 1, when taking into consideration the tension-compression asymmetry (polarization) on the formation of twins, the four twins can be formed under compression, while the others cannot be formed without tensile stress at those loading orientations. This result demonstrates that the {332} twins formation tendencies can be estimated roughly by focusing on the asymmetry of twinning shear that can be evaluated from considering the conventional Schmid factor. However, the discrepancy expected from the consideration based on the Schmid factor was also monitored. The formation of {332} twins is limited at a loading orientation of around $-25^\circ \leq \chi \leq -15^\circ$ in the ST specimen, and their formation was not observed in specimens with a loading axis of $\chi > -15^\circ$, despite a small amount of twins being observed in the specimen with $[\bar{1} \ 4 \ 4.5]$ loading orientation ($\chi = 25^\circ$). The largest Schmid factor for {332} twins among the twelve systems was 0.425^c at $[\bar{1} \ 4 \ 51]$ ($\chi = -25^\circ$) and 0.472^c at $[\bar{1} \ 4 \ 18]$ ($\chi = -15^\circ$) loading orientations, as shown in Table 1. It is to note, however, that at other loading orientations at $\chi > -15^\circ$, some {332} twins maintained relatively high Schmid factors; 0.476^c at $[\bar{1}49]$ ($\chi = 0^\circ$), 0.420^c at $[\bar{1} \ 4 \ 5.8]$ ($\chi = 15^\circ$), and 0.354^c at $[\bar{1} \ 4 \ 4.5]$ ($\chi = 25^\circ$). As described above, the yield stress of the Ti-29Nb-13Ta-4.6Zr crystal showed little orientation dependence. As the slip plane of the $\langle 111 \rangle$ dislocation varied nearly along the MRSSP, the Schmid factor for the $\langle 111 \rangle$ slip must maintain high values of ~ 0.48 – 0.50 at all loading orientations. This implies that the critical resolved shear stress (CRSS) for the $\langle 111 \rangle$ slip varies very little with the loading orientation. Thus, under the Schmid factor-derived consideration, the formation of {332} twins was expected at all investigated loading orientations. However, this differed from the experimental results, indicating that the CRSS for the formation of {332} twins does not obey the Schmid law perfectly, and orientation dependence must be exhibited. Related assumptions have been reported previously by Hanada *et al.* in other alloy systems^{16–18}.

Another notable point is that the differences in orientation dependence of yield stress with heat treatment conditions. As shown in Fig. 6(b), the orientation dependence of the yield stress was negligibly small in the specimens annealed at 598 K in which the ω -phase was precipitated, as similarly to that in the ST specimens, at the loading orientations where $\langle 111 \rangle$ dislocations were operative. On the other hand, the yield stress of the specimens annealed at 723 K in which the α -phase was precipitated tended to show a slight decrease as decreasing in

the χ -value; i.e. the isotropic plasticity degenerated with the presence of α -phase. In the specimens annealed at 723 K, the motion of dislocation was confirmed to control the deformation behavior at all loading orientations, but the variation in the orientation dependence of the yield stress exhibited the “inverse” trend compared to those observed in conventional bcc-metals as described above. As shown in Figs 2 and 4, the morphology of the slip traces in the specimens annealed at 723 K was also largely different from those in the ST specimens and those annealed at 598 K. These results imply that the interacting behaviors of $\langle 111 \rangle$ dislocations with ω - and α -precipitates are different, and a different deformation mechanism will exist and control the mechanical properties of the specimens in which α -phases were precipitated, compared to those in the ST specimens and ω -phase precipitated specimens. Further experimental data are required to discuss such mechanisms, and studies are ongoing in our group.

It was previously reported that the operative deformation mode in the β -Ti alloy varies depending on the β -phase stability governed by the alloy composition and heat-treatment condition^{17,18,23}. In the alloy exhibiting low β -phase stability, the $\{332\}$ twins tend to be operative. The lattice modulation plays a key role in facilitating the formation of the $\{332\}$ twin, and it is enhanced in unstable β -Ti alloys²⁴. While in β -Ti alloys with high β -phase stability, the $\langle 111 \rangle$ slip operation became the dominant deformation mode. The present study clarified that the dominant operative deformation mode varied with loading orientation in the Ti-29Nb-13Ta-4.6Zr alloy single crystals, different from the behavior in Ti-15Mo-5Zr-3Al single crystal²¹. This indicated that β -phase stability in this alloy is the intermediate where the operative deformation mode changes. It was previously reported that the $\{332\}$ twin operation is beneficial for increasing alloy elongation, although it accompanies a reduction in yield stress, and contradictory properties result from slip operations, i.e., an increase in yield stress accompanied by a reduction in ductility²⁵. Thus, the simultaneous twin and slip operations in polycrystalline alloys must be beneficial to ensure both the strength and ductility of the alloy, as pointed out by Min *et al.*²⁶. Furthermore, the increase in the number of operative deformation modes is beneficial for increasing the deformability of the polycrystalline alloy by ensuring that the Mises criterion is met. This accounts for the Ti-29Nb-13Ta-4.6Zr alloy exhibiting good mechanical properties with superior strength and ductility.

In conclusion, the plastic deformation behavior of Ti-29Nb-13Ta-4.6Zr alloy single crystal was first clarified in this study. The $\langle 111 \rangle$ slip and $\{332\}$ twin were identified to be the operative deformation modes. Their operations showed strong crystal orientation dependence, but the resultant variation in yield stress was not significant. That is, the Ti-29Nb-13Ta-4.6Zr alloy single crystal was found to show relatively isotropic plastic properties, which is contradict to its strongly anisotropic elastic properties. This “plastically almost-isotropic and elastically highly-anisotropic” nature is desirable for the development of ‘single crystalline β -Ti implant’ as new hard tissue replacements for suppressing the stress shielding while maintaining the high mechanical reliability.

Method

Fabrication of single crystalline specimens. A mother alloy with a composition of Ti-29Nb-13Ta-4.6Zr (mass%) was supplied by Daido Steel Co. Ltd., Japan. It was prepared by vacuum arc remelting and subsequent forging. From the ingot, single crystals were grown in a furnace (SCI-MDH 20020, Canon machinery, Japan) using the optical floating zone (FZ) method, with a crystal growth rate of 2.5 mm/h, under a flow of high purity Ar gas. In order to ensure the homogeneity of the single crystal composition, the mother ingot and the obtained single crystals were rotated (6 rpm) at opposite directions to each other during crystal growth. Following the crystal growth process, the single crystal was slowly cooled to room temperature (RT, 293 K) over 40 h.

The chemical compositions of the mother ingot and the single crystal were determined by inductively coupled plasma (ICP) analysis and by the inert gas fusion method. As a result, it was confirmed that the chemical composition of the obtained single crystal was confirmed to be comparable to that of the mother alloy for all constituent elements in the quaternary system, with low O concentration (see Supplementary Table S2). The obtained single crystal was subjected to solution treatment (ST) at 1063 K for 3.6 ks under Ar atmosphere, followed by water quenching (WQ). Some crystals were encapsulated once again and annealed at varying temperatures (573, 598, 673, and 723 K) for 259.2 ks, followed by WQ, to provide microstructural variation in the β -phase single crystals. The constituent phase was identified by transmission electron microscopy (TEM, JEM-3010, JEOL, Japan).

Examination of mechanical properties. Compression tests were performed to examine the mechanical properties at RT. Rectangular specimens ($2.0 \times 2.0 \times 5.0$ mm³) were cut by electric discharge machining. After mechanical polishing with SiC paper (#400–2000), the specimens were electropolished in a perchloric acid/butanol/methanol solution 6/35/59 (vol.%). Single crystal orientation was determined using the X-ray back Laue diffraction method with an accuracy of 1°. The loading axis orientation of the compressive specimens was mainly chosen to be $[\bar{1}49]$ where the Schmid factor of the $(\bar{1}01)[111]$ primary slip system had a maximum value of 0.500. Other specimens with four different loading axes were also prepared in a $[001]$ - $[011]$ - $[\bar{1}11]$ standard stereographic triangle as shown in Fig. 4(m), to examine the orientation dependence of the plastic behavior.

Compression tests were conducted on an Instron-type mechanical testing machine (Autograph AG-5000C, Shimadzu, Japan) at a nominal strain rate of 1.67×10^{-4} s⁻¹ under vacuum at RT. Slip markings introduced in the deformed specimens were observed using an optical microscope (OM, BX60M, Olympus, Japan) equipped with Nomarski interference contrast. The slip plane of the dislocations was determined by the two-face slip trace analysis using the OM, and its transition depending on the loading orientation was quantitatively analyzed by the so-called ψ - χ curve method. Deformation structures in the compressed specimens were observed in a TEM operated at 300 kV.

References

- Niinomi, M. Biologically and mechanically biocompatible titanium alloys. *Mater. Trans.* **49**, 2170–2178 (2008).
- Geetha, M., Singh, A. K., Asokamani, R. & Gogia, A. K. Ti based biomaterials, the ultimate choice for orthopaedic implants—A review. *Prog. Mater. Sci.* **54**, 397–425 (2009).
- Niinomi, M. Recent metallic materials for biomedical applications. *Metall. Mater. Trans. A* **33A**, 477–486 (2002).
- Huiskes, R., Weinans, H. & Van Rietbergen, B. The relationship between stress shielding and bone resorption around total hip stems and the effects of flexible materials. *Clin. Orthop. Relat. Res.* **274**, 124–134 (1992).
- Rho, J.-Y., Tsui, T. Y. & Pharr, G. M. Elastic properties of human cortical and trabecular lamellar bone measured by nanoindentation. *Biomaterials* **18**, 1325–1330 (1997).
- Gomes, C. C. *et al.* Assessment of the genetic risks of a metallic alloy used in medical implants. *Gen. Mole. Biology* **34**, 116–121 (2011).
- Long, M. & Rack, H. J. Titanium alloys in total joint replacement—a materials science perspective. *Biomaterials* **19**, 1621–1639 (1998).
- Disegi, J. A., Kennedy, R. L. & Pilliar, R. *Standard specification for wrought titanium-13 niobium-13 zirconium alloy for surgical implant applications* (ed. ASTM) 1071–1077 (ASTM Designation for Biomedical Applications, 2000).
- Kuroda, D. *et al.* Design and mechanical properties of new β type titanium alloys for implant materials. *Mater. Sci. Eng. A* **243**, 244–249 (1998).
- Hao, Y. L. *et al.* Aging response of the Young's modulus and mechanical properties of Ti-29Nb-13Ta-4.6Zr for biomedical applications. *Metall. Mater. Trans.* **33A**, 1007–1012 (2002).
- Niinomi, M. *et al.* Corrosion wear fracture of new β type biomedical titanium alloys. *Mater. Sci. Eng. A* **263**, 193–199 (1999).
- Niinomi, M. Fatigue performance and cyto-toxicity of low rigidity titanium alloy, Ti-29Nb-13Ta-4.6Zr. *Biomaterials* **24**, 2673–2683 (2003).
- Wu, S. *et al.* Biomimetic porous scaffolds for bone tissue engineering. *Mater. Sci. Eng. R* **80**, 1–36 (2014).
- Tane, M. *et al.* Peculiar elastic behavior of Ti-Nb-Ta-Zr single crystals. *Acta Mater.* **56**, 2856–2863 (2008).
- Tane, M. *et al.* Low Young's modulus of Ti-Nb-Ta-Zr alloys caused by softening in shear moduli c' and c_{44} near lower limit of body-centered cubic phase stability. *Acta Mater.* **58**, 6790–6798 (2010).
- Hanada, S. & Izumi, O. Deformation of metastable beta Ti-15Mo-5Zr alloy single crystals. *Metall. Trans. A* **11A**, 1447–1452 (1980).
- Hanada, S., Takemura, A. & Izumi, O. The mode of plastic deformation of β Ti-V alloys. *Trans. Japan Inst. Metals* **23**, 507–517 (1982).
- Hanada, S., Ozeki, M. & Izumi, O. Deformation characteristics in β phase Ti-Nb alloys. *Metall. Trans. A* **16A**, 789–795 (1985).
- Nakano, T. *et al.* Crystal growth and plastic deformation behavior of Ti-29Nb-13Ta-4.6Zr bcc-based single crystal. In: *Ti-2007 Science and Technology, Proc. of the 11th World Conf. on Titanium* 1437–1439 (The Japan Institute of Metal, Sendai, Japan, 2007).
- Akahori, T. *et al.* Improvement in fatigue characteristics of newly developed beta type titanium alloy for biomedical applications by thermo-mechanical treatments. *Mater. Sci. Eng. C* **25**, 248–254 (2005).
- Lee, S. H., Hagihara, K. & Nakano, T. Microstructural and orientation dependence of the plastic deformation behavior in β -type Ti-15Mo-5Zr-3Al alloy single crystals. *Metall. Trans. A* **43A**, 1588–1597 (2012).
- Duesbery, M. S. & Vitek, V. Plastic anisotropy in b.c.c. transition metals. *Acta Mater.* **46**, 1481–1492 (1998).
- Ahmed, M. *et al.* The influence of β phase stability on deformation mode and compressive mechanical properties of Ti-10V-3Fe-3Al alloy. *Acta Mater.* **84**, 124–135 (2015).
- Tobe, H., Kim, H. Y., Inamura, T. & Hosoda, H. Origin of {332} twinning in metastable β -Ti alloys. *Acta Mater.* **64**, 345–355 (2014).
- Hanada, S. & Izumi, O. Correlation of tensile properties, deformation modes, and phase stability in commercial β -phase titanium alloys. *Metall. Trans. A* **18A**, 265–271 (1987).
- Min, X. H., Tsuzaki, K., Emura, S. & Tsuchiya, K. Enhancement of uniform elongation in high strength Ti-Mo based alloys by combination of deformation modes. *Mater. Sci. Eng. A* **528**, 4569–4578 (2011).

Acknowledgements

This work was supported by Grants-in-Aid for Scientific Research (S) from the Japan Society for Promotion of Science (Grant No. 25220912) and by research grants from the Light Metals Educational Foundation of Japan, and the Japan titanium society. This work was also supported by Council for Science, Technology and Innovation (CSTI), Cross-Ministerial Strategic Innovation Promotion Program (SIP), Innovative design/manufacturing technologies (Establishment and Validation of the base for 3D Design & Additive Manufacturing Standing on the Concepts of “Anisotropy” & “Customization”) from the New Energy and Industrial Technology Development Organization (NEDO).

Author Contributions

K.H. and T.N. designed the study and drafted the manuscript. K.H. and H.M. performed the experiments. K.H., H.M. and T.N. analyzed the data. Y.U. and M.N. supervised the work and provided the critical feedback on the manuscript. All authors contributed to discussion of the results.

Additional Information

Supplementary information accompanies this paper at <http://www.nature.com/srep>

Competing financial interests: The authors declare no competing financial interests.

How to cite this article: Hagihara, K. *et al.* Isotropic plasticity of β -type Ti-29Nb-13Ta-4.6Zr alloy single crystals for the development of single crystalline β -Ti implants. *Sci. Rep.* **6**, 29779; doi: 10.1038/srep29779 (2016).



This work is licensed under a Creative Commons Attribution 4.0 International License. The images or other third party material in this article are included in the article's Creative Commons license, unless indicated otherwise in the credit line; if the material is not included under the Creative Commons license, users will need to obtain permission from the license holder to reproduce the material. To view a copy of this license, visit <http://creativecommons.org/licenses/by/4.0/>